

Magnetic control of a meta-molecule

Gavin B. G. Stenning,^{1,*} Graham J. Bowden,¹ Lewis C. Maple,¹ Simon A. Gregory,¹ Alberto Sposito,² Robert W. Eason,² Nikolay I. Zheludev,² and Peter A. J. de Groot¹

¹School of Physics and Astronomy, University of Southampton, SO17 1BJ, UK

²Optoelectronics Research Centre, University of Southampton, SO17 1BJ, UK

*gbs1g09@soton.ac.uk

Abstract: Metamaterials offer the prospect of new science and applications. They have been designed by shaping or changing the material of the individual meta-molecules to achieve properties not naturally attainable. Composite meta-molecules incorporating a magnetic component offer new opportunities. In this work we report on the interaction between a non-magnetic split ring resonator (SRR) and a thin film of yttrium iron garnet (YIG). Strong hybridized resonances are observed. While the SRR is characterized by a magnetic and electric resonance, in practice, it is found that the YIG couples strongly to this symmetric (electric) mode of the SRR. It is also demonstrated that the anti-crossing region provides fertile ground for the creation of elementary excitations such as backward volume magnetostatic waves.

© 2013 Optical Society of America

OCIS codes: (160.3918) Metamaterials; (160.3918) Magneto-optical materials; (230.7370) Waveguides, planar.

References and links

1. R. A. Shelby, D. R. Smith, and S. Schultz, "Experimental verification of a negative index of refraction," *Science* **292**(5514), 77–79 (2001).
2. D. Schurig, J. J. Mock, B. J. Justice, S. A. Cummer, J. B. Pendry, A. F. Starr, and D. R. Smith, "Metamaterial electromagnetic cloak at microwave frequencies," *Science* **314**(5801), 977–980 (2006).
3. J. B. Pendry, A. J. Holden, D. J. Robbins, and W. J. Stewart, "Magnetism from conductors and enhanced nonlinear phenomena," *IEEE Trans. Microw. Theory Tech.* **47**(11), 2075–2084 (1999).
4. M. A. Abdalla and Z. Hu, "Compact and tunable metamaterial antenna for multi-band wireless communication applications," in *2011 IEEE International Symposium on Antennas and Propagation (APSURSI)* (IEEE, 2011), pp. 1054–1057.
5. L. Kang, Q. Zhao, H. Zhao, and J. Zhou, "Magnetically tunable negative permeability metamaterial composed by split ring resonators and ferrite rods," *Opt. Express* **16**(12), 8825–8834 (2008).
6. J. N. Gollub, J. Y. Chin, T. J. Cui, and D. R. Smith, "Hybrid resonant phenomena in a SRR/YIG metamaterial structure," *Opt. Express* **17**(4), 2122–2131 (2009).
7. S. Haroche and J. M. Raimond, "Exploring the quantum: Atoms, Cavities and Photons," (Oxford University Press, 2006).
8. H. Huebl, C. Zollitsch, J. Lotze, F. Hocke, M. Greifenstein, A. Marx, R. Gross, and S. T. B. Goennenwein, "High cooperativity in coupled microwave resonator ferrimagnetic insulator hybrids," arXiv:1207.6039v1 [quant-ph] (25 Jul 2012).
9. A. G. Gurevich and G. A. Melkov, *Magnetization Oscillations and Waves* (CRC Press, 1996).
10. F. Martín, F. Falcone, J. Bonache, R. Marqués, and M. Sorolla, "Miniaturized coplanar waveguide stop band filters based on multiple tuned split ring resonators," *IEEE Microw. Wireless Compon. Lett.* **13**(12), 511–513 (2003).
11. F. Falcone, F. Martín, J. Bonache, R. Marqués, and M. Sorolla, "Coplanar waveguide structures loaded with split-ring resonators," *Microw. Opt. Technol. Lett.* **40**, 3–6 (2004).
12. C. Saha, J. Y. Siddiqui, and Y. M. M. Antar, "Square split ring resonator backed coplanar waveguide for filter applications," in *2011 XXXth URSI General Assembly and Scientific Symposium* (2011), pp. 1–4.
13. R. A. Shelby, D. R. Smith, S. C. Nemat-Nasser, and S. Schultz, "Microwave transmission through a two-dimensional, isotropic, left-handed metamaterial," *Appl. Phys. Lett.* **78**(4), 489–491 (2001).
14. R. W. Eason, *Pulsed Laser Deposition of Thin Films-Applications-Led Growth of Functional Materials* (Wiley Interscience, 2007).

15. C. L. Sones, M. Feinaeugle, A. Sposito, B. Gholipour, and R. W. Eason, "Laser-Induced Forward Transfer-printing of focused ion beam pre-machined crystalline magneto-optic yttrium iron garnet micro-discs," *Opt. Express* **20**(14), 15171–15179 (2012).
 16. H. Zhao, J. Zhou, L. Kang, and Q. Zhao, "Tunable two-dimensional left-handed material consisting of ferrite rods and metallic wires," *Opt. Express* **17**(16), 13373–13380 (2009).
 17. J. M. L. Beaujour, A. D. Kent, D. W. Abraham, and J. Z. Sun, "Ferromagnetic resonance study of polycrystalline $\text{Fe}_{1-x}\text{V}_x$ alloy thin films," *J. Appl. Phys.* **103**(7), 07B519 (2008).
 18. C. Kittel, *Introduction To Solid State Physics*, 8th ed. (Wiley, 2005).
 19. P. He, J. Gao, C. T. Marinis, P. V. Parimi, C. Vittoria, and V. G. Harris, "A microstrip tunable negative refractive index metamaterial and phase shifter," *Appl. Phys. Lett.* **93**(19), 193505 (2008).
 20. D. R. Smith, D. C. Vier, T. Koschny, and C. M. Soukoulis, "Electromagnetic parameter retrieval from inhomogeneous metamaterials," *Phys. Rev. E Stat. Nonlin. Soft Matter Phys.* **71**(3 3 Pt 2B), 036617 (2005).
 21. L. R. Walker, "Resonant modes of ferromagnetic spheroids," *J. Appl. Phys.* **29**(3), 318–323 (1958).
 22. J. F. Dillon, Jr., "Magnetostatic modes in disks and rods," *J. Appl. Phys.* **31**(9), 1605–1614 (1960).
 23. R. W. Damon and J. R. Eshbach, "Magnetostatic modes of a ferromagnet slab," *J. Phys. Chem. Solids* **19**(3-4), 308–320 (1961).
 24. T. Koschny, M. Kafesaki, E. N. Economou, and C. M. Soukoulis, "Effective medium theory of left-handed materials," *Phys. Rev. Lett.* **93**(10), 107402 (2004).
 25. M. Lu, J. Y. Chin, R. Liu, and T. J. Cui, "A microstrip phase shifter using complementary metamaterials," in *International Conference on Microwave and Millimeter Wave Technology, 2008. ICMMT 2008* (IEEE, 2008), pp. 978–980.
 26. B. Luk'yanchuk, N. I. Zheludev, S. A. Maier, N. J. Halas, P. Nordlander, H. Giessen, and C. T. Chong, "The Fano resonance in plasmonic nanostructures and metamaterials," *Nat. Mater.* **9**(9), 707–715 (2010).
 27. H. How, P. Shi, C. Vittoria, L. C. Kempel, and K. D. Trott, "Single-crystal YIG phase shifter using composite stripline structure at X band," *J. Appl. Phys.* **87**(9), 4966–4968 (2000).
-

1. Introduction

Metamaterials are man-made patterned structures which exhibit unusual electromagnetic properties. In recent years, this subject has developed into a rich research field, motivated by the promise of both ground-breaking science and device applications. It is possible to engineer metamaterials with a negative index of refraction [1], and to achieve ‘cloaking’ at microwave frequencies [2]. Such desirable properties are achieved at frequencies close to the resonances of the so called *meta-molecule* that comprise the metamaterial.

To date, most research has concentrated on manipulating relatively simple materials such as ohmic metals and low-loss dielectrics. The most commonly employed meta-molecule is the split ring resonator (SRR), a system which has been extensively studied ever since the original proposal by Pendry *et al.* [3]. A given metamaterial consists of a periodic array, in our case SRRs, providing a collective response to an electromagnetic wave. However, such systems are often restricted to a narrow frequency band due to the resonant character of the individual meta-molecule. To overcome this limitation, attention has therefore turned to tunable metamaterials.

In this paper, we report on composite structures containing active magnetic components. In particular, we discuss a hybrid structure which incorporates a high-conductivity SRR and a thin film of insulating yttrium iron garnet (YIG). In essence, there are two differing resonances to be considered: that of the SRR and that of the YIG. Since the latter is field-dependent, tunability of the composite structure can be achieved using an applied magnetic field. Consequently, the transmission can therefore be controlled, as required. Tunability of magnetic resonances in the microwave regime offers a powerful means to realize controllable, loss-compensating, multi-frequency antennas [4].

Kang *et al.* [5] were the first to report a magnetically tunable metamaterial, made up from an SRR array and small rods of YIG, all placed in an X-band waveguide. The resulting complex resonances were subsequently interpreted by Gollub *et al.* [6]. Our research centers on the interaction between a thin (2.4 μm) YIG film and a single SRR, excited by a broadband co-planar waveguide (CPW). The results show that strong hybridization occurs between the SRR and YIG resonances. The latter is interpreted using a simple two-state model, for an SRR and YIG film respectively [7,8]. In addition, it is argued that the non-

linear interaction between the SRR and YIG provides a fertile breeding ground for the excitation of spin-waves, magnetostatic surface wave (MSSW) and backwards volume magnetostatic wave (BVMSW) [9]. In practice, Spin-waves, MSSWs and BVMSWs are easily incorporated into the two-state model.

2. Experimental arrangement

We turn now to the experimental arrangement used in this work. Martin *et al.* [10] and Falcone *et al.* [11] have shown that resonances in SRR systems can be studied and exploited in a co-planar arrangement, in close proximity to a broadband coplanar waveguide (CPW). Such an arrangement presents increased opportunities for applications as a broadband tunable device. Further, it is found that SRRs placed on the reverse side of the CPW substrate couple effectively to the CPW, resulting in lower transmission losses, while still revealing strong metamaterial resonances [12]. Schematic diagrams, showing the physical arrangement of the CPW, SRRs, and the YIG film used in this work, can be seen in Fig. 1. This arrangement possesses extensive advantages. The planar geometry is suited to applications and only small quantities of YIG are required.

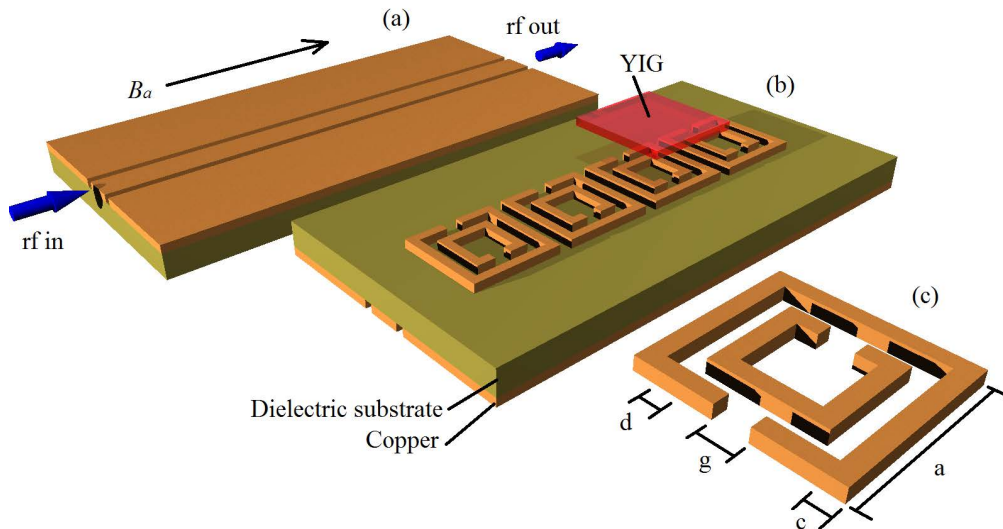


Fig. 1. Schematic view of a) Top view of the CPW. b) SRRs (metamaterial) located on the underside of the CPW substrate. The YIG film is placed directly on top of one SRR. c) Single split ring resonator (SRR). Dimensions of, $a = 3.93$ mm, $c = 0.375$ mm, $d = 0.45$ mm, $g = 0.69$ mm. Field direction as shown by B_a .

The applied magnetic field was supplied by an electromagnet, driven by a computer-controlled DC bipolar power supply. The magnetic field strength was recorded using a Lakeshore 425 Gaussmeter. The rf field, applied perpendicular to the DC field, was delivered by a 20 GHz vector network analyzer (VNA) (HP E5071C) through low loss broadband cables. The cables were inserted through the centre of the electromagnet pole pieces and connected to the coplanar waveguide (CPW) using end launch connectors. The signal line width and gap size is set at 1.1 mm and 200 μ m respectively, as shown in Fig. 1(a), which allows the CPW to be a broadband frequency device in the range 1-20 GHz with the required 50Ω impedance. The VNA provides a frequency sweep from 300 kHz to 20 GHz while simultaneously monitoring microwave transmission over this range. In summary, the CPW provides the rf field to the overall system, exciting both the SRR and YIG film, simultaneously. Hence a transverse electromagnetic geometry is achieved. More details of the SRR can be seen in Fig. 1(b) and (c). The SRR is fabricated on the underside of the

CPW, directly underneath one of the signal lines in order to maximize rf-coupling [11]. The CPW itself was fabricated using a simple mask/photo-etching technique. A 70 μm copper layer on both sides of a 0.7 mm thick dielectric sheet was used as the substrate (FR4, $\epsilon_r = 4.5$). The SRR, fabricated on the reverse of the CPW with dimensions specified in Fig. 1(c), is similar to the design by Shelby *et al.* [13]. However, the dimensions of the SRR have been modified to produce frequencies close to the ferrimagnetic resonance (FMR) of the YIG, in the available magnetic field range 0-0.5 T.

The YIG film was grown on a single crystal yttrium aluminum garnet (100 oriented) substrate by pulsed laser deposition using a KrF excimer laser operating at 248 nm [14,15]. YIG was used as the magnetic component in this experiment, because (*i*) it possesses a strong narrow line-width FMR, (*ii*) it is characterized by negative permeability on resonance [16], and (*iii*) there are no complications from eddy current losses. The YIG film was placed directly on top of the SRR (flip-chip method) [17], thus allowing strong coupling to the CPW and therefore good microwave excitation. The VNA allows for collection of the S-matrix parameters, including the transmission coefficient S_{21} . The latter describes the transmission properties of the combined SRR, YIG film and CPW.

3. Experimental results

The results presented here are for a single SRR as this avoids the complex effects reported by Kang *et al.* [5] associated with cells at the boundaries of the array. Results were also obtained using an array of 4 SRRs and a YIG film. The results proved similar to those presented here but with a frequency shift from the meta-molecule resonance. The S_{21} transmission was measured in a frequency vs field map (ν - B_a), in the range 1-20 GHz and 0-0.38 T. In Fig. 2 the color at a given point in the map represents the magnitude of S_{21} . In addition, it should be

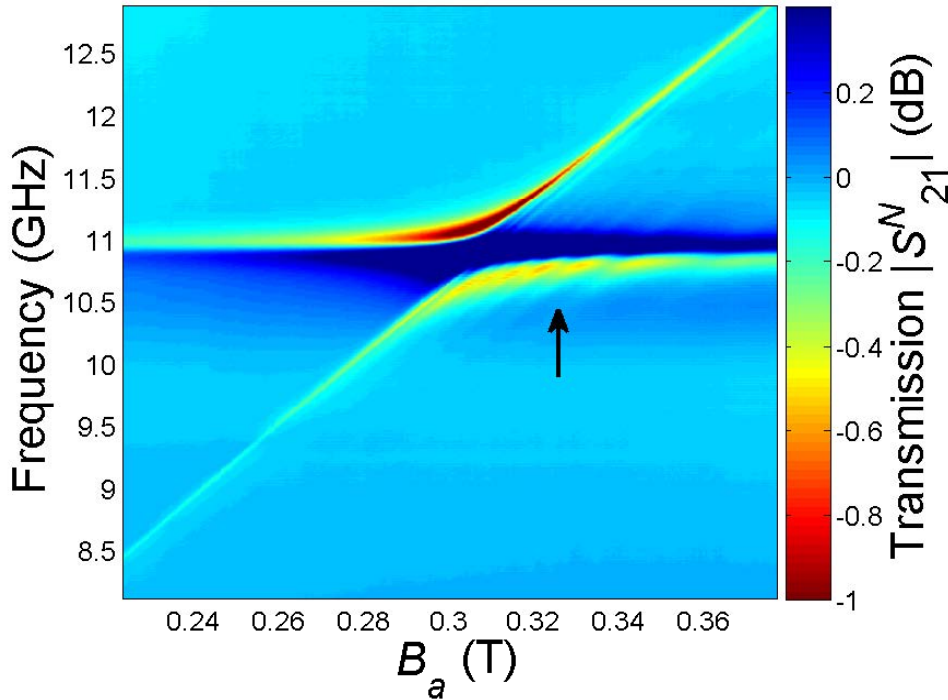


Fig. 2. The (ν - B_a) map of the YIG-SRR anti-crossing modes. The transmission colour-bar on the right represents transmission (positive values/blue) and absorption (negative values/red). Satellites of the FMR are visible to the right of the anti-crossing and FMR shown by the black arrow. These arise from the creation of BVMSWs.

noted that the following S_{21} map plots shown were normalized, by subtracting the S_{21} transmission obtained in a small (approximately zero) magnetic field ($B_a = 0.001$ T) from every subsequent frequency sweep. This gives a final value of $|S_{21}^N|$, leaving only field dependent features in the resulting plot. Such maps clearly show (i) the individual SRR and YIG resonances, and (ii) strong anti-crossing behavior, when the two resonances coincide. SRRs of various sizes were used.

The normalized S_{21}^N map of the CPW/SRR/YIG composite system in Fig. 2 covers a reduced frequency (8.0-13 GHz) and magnetic field range (0.22-0.38 T); this then draws attention to the hybridization between the SRR and YIG resonances. The diagonal line, from the bottom left to the top right, is the expected YIG FMR absorption. For this mode, the frequency versus field follows the usual Kittel formula [18]. The SRR resonance appears as a horizontal line at 10.9 GHz. At that point where the YIG and SRR resonances are expected to cross, strong anti-crossing behavior occurs. In particular, at the SRR resonance at $\nu = 10.9$ GHz, and it is seen that there is a reduction in microwave losses on resonance at a field of $B_a = 0.3$ T. This point is illustrated in Figs. 2 and 3 at the centre of the anti-crossing. Above and below the anti-crossing (black and blue curves respectively in Fig. 3) there are absorption troughs (negative) associated with the field-dependent YIG FMR, while exactly at the centre of the anti-crossing, there is a large reduction in the losses amounting to 1.6 dB (peak). This is indicative of an effective negative index of refraction, as obtained by He *et al.* [19], using the experimental S-parameter retrieval technique [20]. Finally, note the presence of satellites on the high field side of the transmission peak. These features are due to the excitation of BVMSWs as discussed in [9, 21-23] and in more detail in section 4 below.

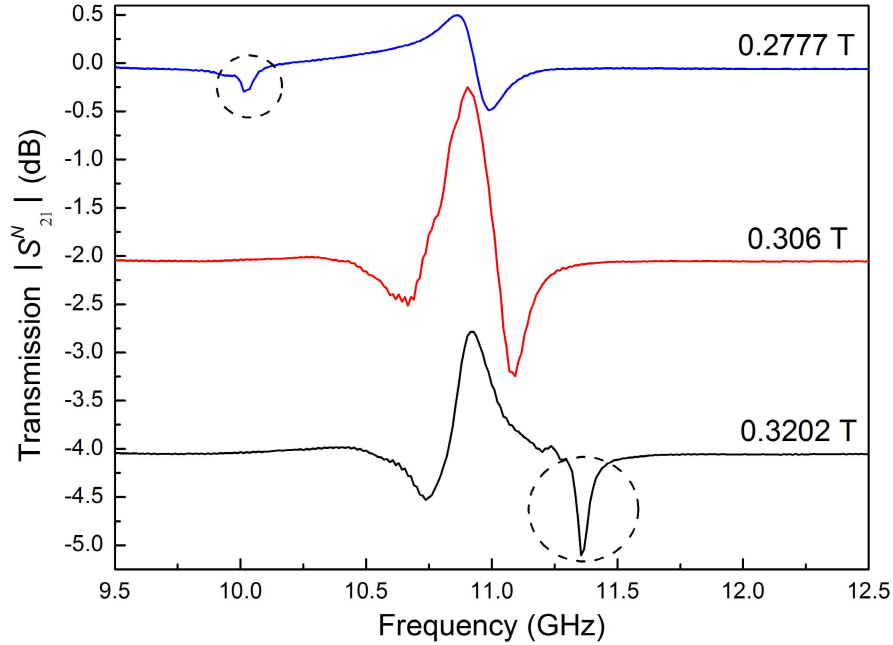


Fig. 3. Normalized transmission S_{21}^N vs frequency (ν) at three fixed fields from Fig. 2 (a) $B_a = 0.2777$ T, (b) 0.306 T and (c) 0.3202 T, blue, red and black respectively. For clarity, each frequency trace is vertically offset by 2 dB.

The resonances shown in Fig. 3, are similar to those described theoretically by Gollub *et al.* [6]. The low frequency trough of trace $B_a = 0.2777$ T is the FMR resonance while the high frequency peak is associated with the symmetric electric-dipole resonance of the SRR. This

has been confirmed experimentally by shorting the gaps in the ring with a short strip of conducting wire, following Ref. [24]. This procedure eliminates the low frequency anti-symmetric magnetic resonance of the SRR at ~ 5 GHz (not shown), while leaving the symmetric electric-dipole resonance response at 10.9 GHz unchanged. Note that as the field is increased the YIG resonance passes through the SRR resonance, distorting the hybridization, as shown in Fig. 3 ($B_a = 0.306$ T) revealing the 1.6 dB reduction in losses. In general, the YIG resonance is no longer visible and the natural resonance of the SRR is observed, on either side of where the FMR would appear. On increasing the applied field still further the YIG resonance moves above that of the SRR resonance. It is also evident, on comparing the curves of $B_a = 0.2777$ T, and 0.3202 T in Fig. 3, that the SRR effective frequency trace is inverted in shape and shifted by 0.25 GHz to a lower frequency ($B_a = 0.3202$) with respect to the first trace of $B_a = 0.2777$. This is in agreement with the observations of Kang *et al.* and Gollub *et al.* [5,6]. A 19.76° phase reversal [25] was also observed over the anti-crossing. This behavior was also found to follow a similar pattern in its reversal to that observed in the absorption $v\text{-}B_a$ map in Fig. 2.

Various orientations of SRR with respect to the direction of the magnetic field were also investigated, and the results of a 90° rotation can be seen in Fig. 4. It is clear that the hybridization/interaction is much stronger for the orientation of the SRR as shown in Fig. 4(b), in particular, transmission at the centre of the anti-crossing, has increased by 1.6 to 4.0 dB. A shift in frequency of 0.25 GHz of the electric dipole resonance is also evident as the YIG FMR passes across. Clearly the orientation of the SRR with respect to the magnetization field is important, if increases in microwave transmission S_{21} are to be achieved. Note also concomitant increases in absorption, on both sides of the anti-crossing as shown by the arrows in Fig. 4(b). The resonance shows a similar form to that of the Fano-resonance [26].

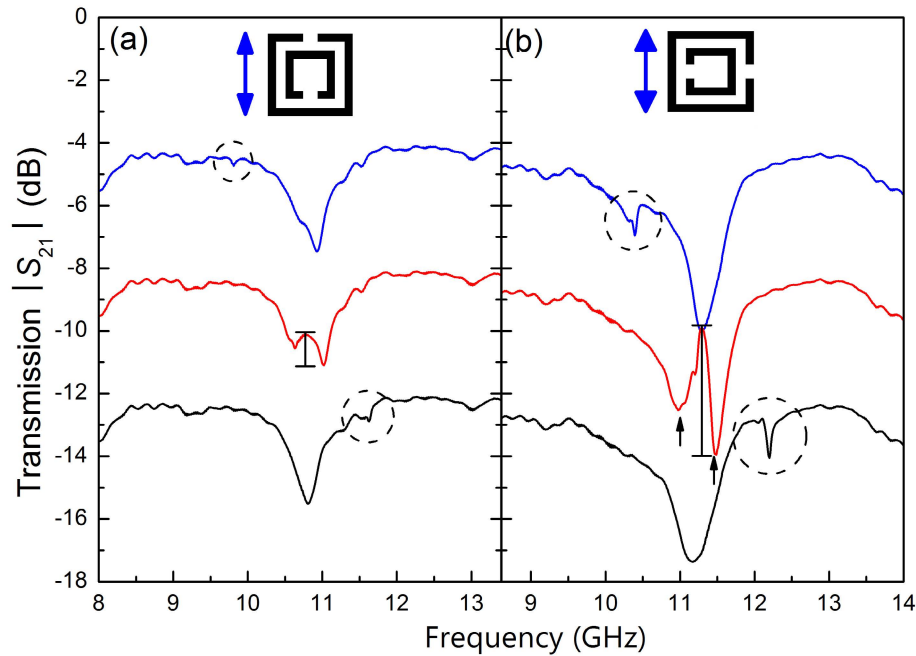


Fig. 4. Unnormalized data (S_{21}) for two orientations of the SRR. The blue arrow represents the electric field polarization as supplied by the CPW. The resonance S_{21} curves blue, red and black were obtained for applied fields of 0.27 T, 0.30 T and 0.33 T, respectively. The dashed circles indicate the YIG resonance, with vertical black lines representing the reduction in microwave losses. Each frequency trace has been offset vertically by 4 dB.

This concludes our broad discussion of the experimental results. We turn now to a theoretical discussion of the anti-crossing and the finer details evident in the S_{21}^N map of Fig. 2.

4. Anti-crossing, spin-waves, magnetostatic surface waves and backwards moving magnetostatic modes

Modeling of the anti-crossing has been performed using the COMSOL modeling package. The results replicate the observed anti-crossing, but with poor resolution due to the need to cover a wide magnetic field and frequency range. Thus more subtle details, such as the observation of BVMSWs, are precluded. However considerable insight into the problem can be gained by adopting the two-state model developed in [7,8], for a SRR in close contact with a YIG film. Following the latter, we assert that the anti-crossing between the resonant frequency of the split-ring and the uniform YIG resonance can be described by a simple 2×2 matrix:

$$\mathbf{M} = \begin{bmatrix} \nu_{SRR} & \delta \\ \delta & \nu_{YIG} \end{bmatrix} \quad (1)$$

Here, ν_{SRR} (ν_{YIG}) is the resonant frequency of the SRR (YIG film) respectively, while δ represents the *mutual interaction* between the split-ring and the YIG film. The YIG resonant frequency for a thin film magnetized in plane is given by

$$\nu_{YIG} = \gamma \sqrt{B_a (B_a + \mu_0 M_0)} \quad (2)$$

where γ and M_0 are the gyromagnetic ratio and saturation magnetization of YIG respectively. So for a finite interaction δ , anti-crossing and mode mixing will occur. This is particularly evident when the diagonal elements of the matrix \mathbf{M} are degenerate (i.e. $\nu_{SRR} \equiv \nu_{YIG}$). Mode mixing of the SRR and YIG resonances then amounts to 50%. In general, the roots of \mathbf{M} are given by

$$\lambda_{\pm} = \frac{1}{2} (\nu_{SRR} + \nu_{YIG}) \pm \frac{1}{2} \sqrt{(\nu_{SRR} - \nu_{YIG})^2 + 4\delta^2} \quad (3)$$

At the anti-crossing center $\lambda_{\pm} = \nu_{SRR} \pm \delta$. Thus the splitting between the two branches is 2δ , which allows a simple measurement of the strength of the interaction between the YIG and the SRR. From the experimental data in Fig. 2, we find $\delta \approx 0.15$ GHz. Further, on using this value together with (i) $\nu_{SRR} = 10.9$ GHz, (ii) $M_0 = 139.26 \times 10^3$ A/m [27] and (iii) $\gamma = 2.949 \times 10^{10}$ (Hz/T) [18], we find the combined response of the SRR and YIG film (solid lines) shown in Fig. 5. From a comparison of the latter with the experimental results of Fig. 2, it is evident that the two-state model describes the anti-crossing behavior very well.

The two-state model is easily modified to take into account the generation of spin-waves and/or non-uniform Walker magnetostatic modes. For a spin-wave or MSSW the YIG resonance is shifted according to

$$\nu_{YIG} = \gamma \sqrt{(B_a + Dk_s^2)(B_a + \mu_0 M_0 + Dk_s^2)} \quad (4)$$

(see Ref. [9]). Here, the energy of the spin-wave is given by $E(k_s) = Dk_s^2$, where D is the spin-wave stiffness factor and k_s the wavenumber. From a comparison of Eqs. (2) and (4) therefore, it is evident that the generation of spin-waves with differing wave-vectors k_s will give rise to a whole host of parallel lines, to the left of the uniform Walker mode. By contrast, the generation of non-uniform volume magnetostatic modes will give rise to a whole host of lines to the right of the uniform Walker mode known as BVMSWs (see Ref. [9], p157 and 165). Unlike spin-waves and MSSWs these are characterized by a negative

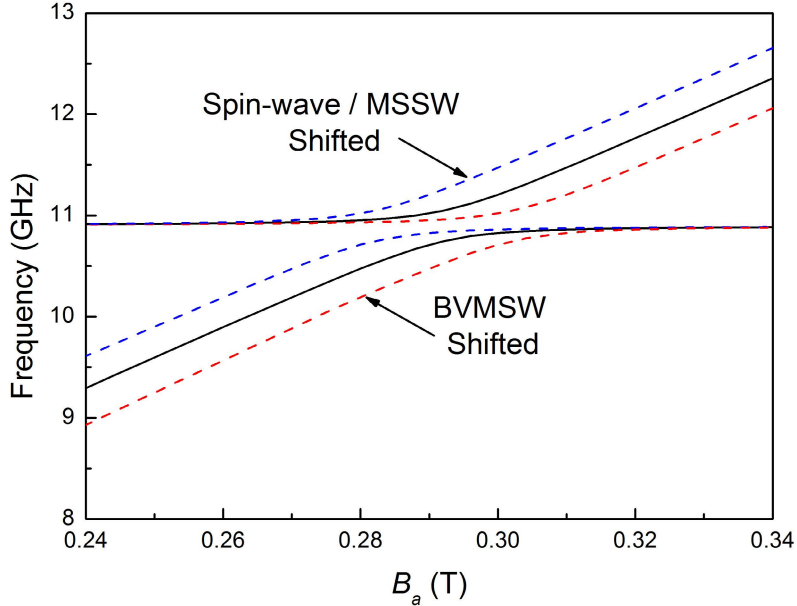


Fig. 5. Anti-crossing of the SRR and YIG modes, obtained using a simple two-level model. Dotted lines show the effects of discrete spin-wave, MSSW and BVMSW excitations.

group velocity $v_g = \partial\omega/\partial k_s < 0$: hence the description ‘backwards’. In practice, the generation of spin-waves, MSSWs or non-uniform Walker modes will be dictated by the geometry and strength of the rf field associated with the SRR. However for the thin YIG sample in question, it is evident that there are a very large number of allowed k -values, given the very large aspect ratio (thickness to width) of the thin film $\sim 1:3 \times 10^3$ (see Refs. [21–23]). To examine this point in more detail therefore, experiments were performed using thicker bulk YIG. The results for a $5 \times 5 \times 0.5$ mm³ thick piece (aspect ratio 1:10) can be seen in Fig. 6. Two new features are immediately apparent. One, the YIG FMR resonance is now dominant over that of the SRR, appearing directly in the anti-crossing region. Two, the discrete nature of the BVMSWs is now very apparent on the right-hand side of the FMR. These are the magnetostatic waves first described by Dillon [22]. Some lines are also apparent on the left-hand side of the FMR. We attribute these lines to the creation of either spin-waves or MSSWs with long wavelengths $\lambda \sim 1$ μm. Clearly the non-linear interaction between the SRR and bulk YIG provides a fertile breeding ground for the excitation of spin-waves, surface magnons and BVMSWs. In practice, it should be possible to generate specific excitations, with well-defined k_s values, using SRRs with tailored shapes, such as those shown in Fig. 1 of Ref. [8]. However, more work will be required to determine the optimum thickness/filling factor of the YIG film, with respect to the dimensions of the SRR. Also the precise form of the rf excitation fields produced by the SRR is important. At the so-called magnetic-mode at ~ 5 GHz, anti-crossing exists but at a much weaker level. The interactions described above are much stronger when the SRR is excited in the symmetric-electric mode ~ 10.9 GHz.

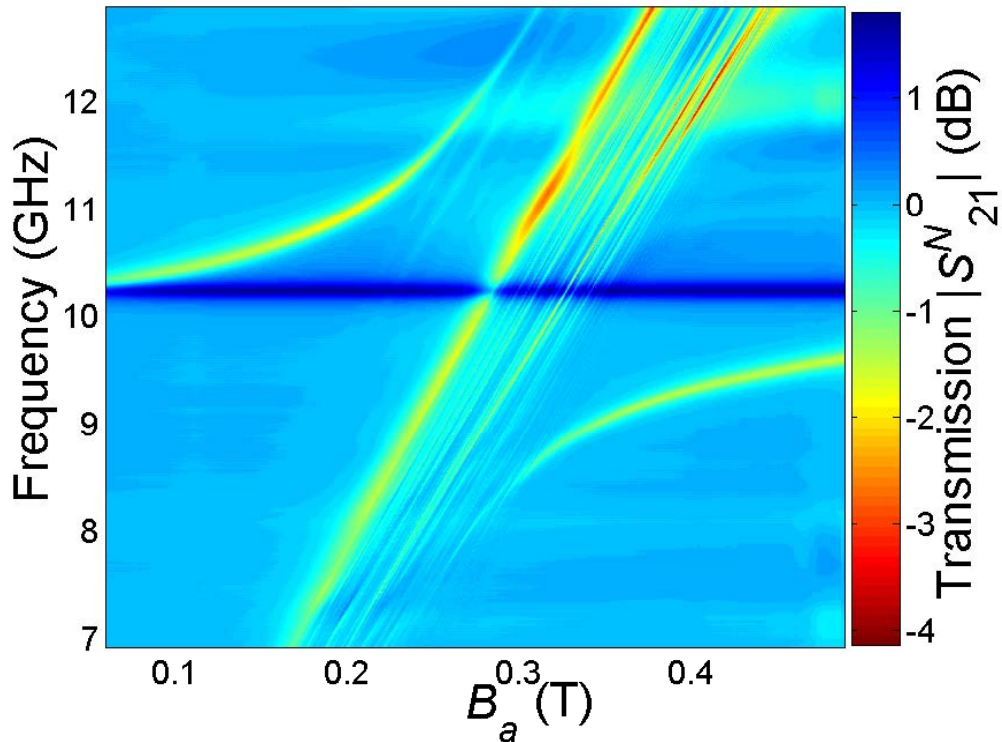


Fig. 6. As per Fig. 2 but with a $5 \times 5 \times 0.5 \text{ mm}^3$ thick bulk YIG crystal.

5. Conclusions

In summary, it has been demonstrated that CPW-based composite SRR metamaterials, incorporating a magnetic component (YIG), can be tuned by applying a magnetic field. The coupling between the SRR and the YIG gives rise to hybridization of the two resonances, yielding a frequency response similar to that of a Fano-resonance [26]. In particular, the anti-crossing regime allows tuning over a frequency range ~ 0.3 GHz, much wider than that of the SRR metamaterial taken in isolation. There is good agreement between experiment with electromagnetic simulations obtained using COMSOL, and the two-state model [7,8]. It has also been demonstrated that the anti-crossing region provides fertile ground for the creation of elementary excitations. Spin-waves, magnetostatic surface waves and backwards volume magneto-static waves have been observed. Finally, it has been shown that the orientation of the SRR with respect to the magnetization of the YIG and CPW is important. In particular, transmission, at the centre of the anti-crossing, could be increased by 1.6 to 4.0 dB, simply by rotating the SRR through 90°. Such experiments demonstrate that tunability is dependent not only on the strength of the magnetic field but also on the orientation of the SRR with respect to the CPW.

Acknowledgment

The authors would like to acknowledge the financial support of the Engineering and Physical Sciences Research Council (U.K.).